

Analysis of supersaturation and nucleation in a moving solution droplet with flowing supercritical carbon dioxide

Mamata Mukhopadhyay* and Sameer V Dalvi

Department of Chemical Engineering, Indian Institute of Technology Bombay, Powai, Bombay 400 076, India

Abstract: A supercritical antisolvent (SAS) process is employed for production of solid nanoparticles from atomized droplets of dilute solution in a flowing supercritical carbon dioxide (SC CO₂) stream by attaining extremely high, very rapid, and uniform supersaturation. This is facilitated by a two-way mass transfer of CO₂ and solvent, to and from the droplet respectively, rendering rapid reduction in equilibrium solubility of the solid solute in the ternary solution. The present work analyses the degree of supersaturation and nucleation kinetics in a single droplet of cholesterol solution in acetone during its flight in a flowing SC CO₂ stream. Both temperature and composition are assumed to be uniform within the droplet, and their variations with time are calculated by balancing the heat and mass transfer fluxes to and from the droplet. The equilibrium solubility of cholesterol with CO₂ dissolution has been predicted as being directly proportional to the Partial Molar Volume Fraction (PMVF) of acetone in the binary (CO₂-acetone) system. The degree of supersaturation has been simulated up to the time required to attain almost zero cholesterol solubility in the droplet for evaluating the rate of nucleation and the size of the stable critical nuclei formed. The effects of process parameters have been analysed in the pressure range of 7.1–35.0 MPa, temperature range of 313–333 K, SC CO₂ flow rate of 0.1136–1.136 mol s⁻¹, the ratio of the volumetric flow rates of CO₂-to-solution in the range of 100–1000, and the initial mole fraction of cholesterol in acetone solution in the range of 0.0025–0.010. The results confirm an extremely high and rapid increase in degree of supersaturation, very high nucleation rates and stable critical nucleus diameter of the order of a nanometre.

© 2005 Society of Chemical Industry

Keywords: supersaturation; nucleation; critical nucleus; partial molar volume fraction; solid solubility; CO₂ dissolution; supercritical antisolvent (SAS)

NOTATION

A	Pre-exponential factor	N_1	Number of moles of CO ₂ in the droplet (kmol m ⁻² s ⁻¹)
B	Parameter for nucleation	N_2	Number of moles of solvent in the droplet (kmol m ⁻² s ⁻¹)
c	Concentration (K mol m ⁻³)	r_c	Size of critical stable nuclei (m)
d	Mean crystal size (m)	S	Degree of supersaturation
D	Diffusivity (m ² s ⁻¹)	T	Temperature (K)
G	Gibbs free energy (J mol ⁻¹)	Δt	Time interval (s)
h	Enthalpy (J mol ⁻¹)	t_e	Time required for complete for removal of solvent (s)
\mathcal{J}	Nucleation rate (number of nuclei m ⁻³ s ⁻¹)	t_0	Time for reduction of equilibrium solubility to zero (s)
k	Boltzmann's constant	v	Molar volume (m ³ kmol ⁻¹)
k_G	Local gas phase mass transfer coefficient (m s ⁻¹)	V_m	Volume of molecule (m ³)
k_L	Local liquid phase mass transfer coefficient (m s ⁻¹)	x_1	CO ₂ mole fraction in ternary liquid mixture
N	Number of condensable molecules (kmol)	X_1	CO ₂ mole fraction in binary (CO ₂ -acetone) liquid mixture
N_A	Avogadro's number	x_3	Cholesterol mole fraction in ternary liquid mixture
N_{Tot}	Total number of moles in the droplet at any time t (kmol)		
N_0	Initial number of moles in the droplet (kmol)		

* Correspondence to: Mamata Mukhopadhyay, Department of Chemical Engineering, Indian Institute of Technology Bombay, Powai, Bombay 400 076, India

E-mail: mm@che.iitb.ac.in

(Received 7 April 2004; revised version received 12 October 2004; accepted 21 October 2004)

Published online 16 February 2005

X_3	Cholesterol mole fraction in acetone on CO ₂ -free basis
α_c	Condensation coefficient
θ	Non-isothermal factor
ρ	Density (kg m ⁻³)
ρ_M	Molar density of solid (kmol m ⁻³)
σ	Surface tension (N m ⁻¹)
ω	Acentric factor

Superscripts

G Gaseous/fluid phase

i Interface

L Liquid phase

* Indicates the equilibrium condition

Subscripts

b Indicates property of the bulk of the solution

diss Indicates the variable related to dissolution

evap Indicates the variable related to evaporation

s Relates to nucleus surface

v Relates to nucleus volume

0 Zero cholesterol solubility

1 CO₂

2 Acetone

3 Cholesterol

1 INTRODUCTION

The supercritical antisolvent (SAS) process entails attainment of extremely high, very rapid and uniform supersaturation of solid solute in the solution droplet during its flight through the CO₂ continuum, owing to a very rapid increase in the antisolvent CO₂ mole fraction in the droplet. This facilitates uniform nucleation and almost instantaneous precipitation, resulting in the formation of ultra-fine particles with a narrow particle size distribution and controlled morphology.¹ The rate of attainment of supersaturation at any instant of time decides the rate of nucleation and the diameter of the stable nucleus, and in turn the size, size distribution and morphology of the particles formed, provided growth and agglomeration can be controlled.

The SAS process can be carried out at two different thermodynamic states, namely, below or above the mixture critical pressure (BMCP or AMCP) for the immiscible or miscible conditions respectively. At the immiscible condition, the antisolvent CO₂ is in the supercritical state and there exists an interface between the droplet and supercritical carbon dioxide (SC CO₂) whereas, at the miscible condition, no interface exists between the droplet and CO₂ at equilibrium. However the solution remains in the liquid phase as a compressed liquid, till it attains a value of CO₂ mole fraction corresponding to the mixture critical point (MCP). In the SAS process the solution is generally very dilute and the fluid-liquid equilibrium compositions of CO₂ and solvent (at the interface) in the binary and ternary systems are not significantly

different.² Also, the solid solute present in the solution is not likely to affect the molar volume of the solution and also the rates of mass transfer of CO₂ and solvent to and from the droplet respectively.

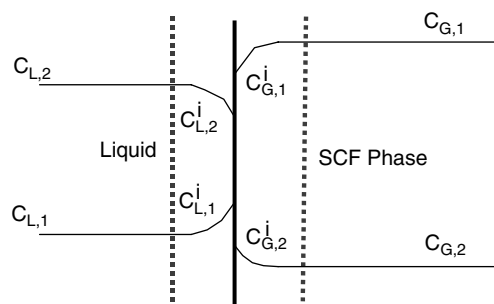
Bristow *et al*³ performed simulation for precipitation of acetaminophen from its ethanol solution using CO₂ at BMCP and AMCP. They reported a maximum attainable supersaturation for which $\ln c/c_0$ was as high as 9. Particle formation by the solution-enhanced dispersion by supercritical fluids (SEDS) process was also modelled based on the concept that the supersaturation was the single most important process parameter for precipitation of acetaminophen from ethanol solution.⁴ Werling and Debenedetti^{5,6} had earlier considered a stagnant solvent droplet of an assumed initial size in a stagnant CO₂ environment at BMCP and an arbitrary droplet radius was defined for the miscible conditions at AMCP. The equations of continuity were solved at isothermal conditions for the CO₂-toluene system. The trend of droplet swelling or shrinking was attributed to the total molar flux to or from the droplet surface. In our earlier work,⁷ the mechanism of SAS was modelled based on simultaneous mass and heat transfer with hydrodynamics of a single atomized droplet of cholesterol solution in flight through a moving SC CO₂ continuum for the BMCP and AMCP conditions of the CO₂-acetone system. Two concentric nozzles having fixed dimensions were considered for spraying of the solution and SC CO₂ with the latter flowing through the annular space. Initial droplet size was calculated at different conditions. The velocity of the droplet during its flight through the SC CO₂ environment was estimated by applying a force balance on the droplet. The temperature and size of the droplet were calculated from the simultaneous heat and mass transfer rates of CO₂ and solvent, total number of moles in the droplet at any instant of time and the molar density of the solution respectively. It was observed that the droplet shrank in the vicinity of the MCP, whereas it swelled at all other conditions far removed from the MCP. The simulation results indicated that a higher temperature, lower pressure, higher mass flow rate of CO₂ and solution or a lower ratio of volumetric flow rates of CO₂-to-solution facilitated formation of a smaller droplet size, faster transport of the solvent and faster increase in the CO₂ mole fraction.⁷

The current paper presents the effects of pressure, temperature, flow rates of CO₂ and solution, and initial solution concentration on the rates of supersaturation and nucleation of cholesterol in a single droplet of acetone solution for both thermodynamic states of BMCP and AMCP. The degree of supersaturation, nucleation rate and critical nucleus size have been analysed in the internally well-mixed non-isothermal single droplet up to t_0 , the time required for the equilibrium cholesterol solubility to become negligible in the droplet.

2 MODEL ASSUMPTIONS

The mechanism of the SAS process entails dissolution of CO₂ at the interface of the droplet with liberation of heat and this heat of dissolution instantaneously causes vaporization of solvent at the interface with an associated change in the bulk temperature of the droplet, depending on the relative rates of mass transfer of solvent vapour and CO₂. It is assumed that the droplet is internally well mixed with uniform temperature and composition within the droplet. The film theory is assumed for the transfer of SC CO₂ and solvent vapour with the corresponding resistances in the liquid film and the fluid film respectively on either side of the interface, as depicted in Fig 1. The liquid and vapour phase concentrations at the interface are assumed to be constrained by the thermodynamic criterion of the fluid–liquid phase equilibrium, which ensures single-phase mass transfer in the individual films on either side of the interface. The concentrations at the interface are calculated from the product of molar density and the corresponding equilibrium mole fractions for BMCP and the MCP mole fractions for AMCP. The driving forces decide the directions and the relative values of the fluxes for solvent and CO₂ during its flight through the CO₂ continuum. The degree of supersaturation attained in the droplet solution is very high, rapid and unstable, causing primary homogeneous nucleation and instantaneous precipitation.

Mass-Transfer Fluxes of CO₂ (1) and Solvent (2)



Heat-Transfer Fluxes

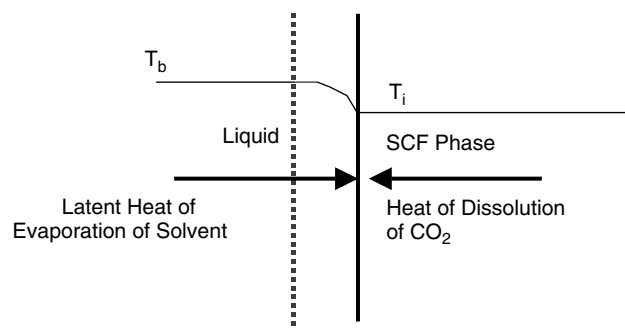


Figure 1. An SAS model for mass and heat transfer fluxes and driving forces.

3 MODEL EQUATIONS

3.1 Composition and temperature of the droplet

The composition of the droplet is calculated from the number of moles of the components present in the droplet at any instant of time. The total number of moles of solution in the droplet at any time is calculated by estimating the fluxes of CO₂ and solvent vapour to and from the droplet respectively at very small intervals of time, Δt (of the order of 10^{-7} – 10^{-4} s). Thus:

$$N_{\text{Tot}} = N_0 + \pi d^2 (N_1 + N_2) \Delta t \quad (1)$$

where N_0 is the initial number of moles in the droplet, d is the diameter of the droplet, N_1 is the flux of CO₂ in $\text{kmol m}^{-2} \text{s}^{-1}$ and N_2 is the flux of solvent vapour in $\text{kmol m}^{-2} \text{s}^{-1}$. The two fluxes are given as:

$$N_1 = k_L (C_{L,1}^i - C_{L,1}) = k_L (\rho_L^i x_1^i - \rho_L x_1) \quad (2)$$

where, C_1^i and x_1^i are the interfacial concentration and liquid phase mole fraction of the CO₂ respectively, and

$$N_2 = k_G (C_{G,2}^i - C_{G,2}) = k_G (\rho_G^i y_2^i - \rho_G y_2) \quad (3)$$

where, C_2^i and y_2^i are the interfacial concentration and fluid phase mole fraction of the solvent respectively. The molar density of the liquid and fluid phases is calculated using the Peng–Robinson equation of state.⁸ The mole fractions at the interface are calculated from solid–liquid–vapour (S–L–V) equilibrium using a recent thermodynamic approach² for the ternary (CO₂–solvent–solid) system from the binary (solvent–CO₂) interaction constants and the solid solubility at a reference pressure.

The temperature of the bulk of the droplet, T_b , is estimated by balancing the heat flux to the interface at temperature T_i (which is the same as that of the fluid phase) and the heat accumulated inside the droplet due to the heat of dissolution of CO₂ in excess of the heat for vaporization of the solvent as:

$$T_b = T_i + (1/h_L)(\Delta h_{\text{diss}} N_1 + \Delta h_{\text{evap}} N_2) \Delta t \quad (4)$$

3.2 Degree of supersaturation

The degree of supersaturation, S , is calculated in this work as the ratio of the mole fractions:

$$S = \left(\frac{x_3}{x_3^*} \right) \quad (5)$$

where x_3 and x_3^* are the actual and the equilibrium mole fractions respectively of the solid solute 3 at the given temperature and pressure condition. x_3 is calculated from the ratio of the number of moles of the solute to the total number of moles of the solution present in the droplet, whereas x_3^* is calculated as a function of CO₂ mole fraction in the solution within the droplet at S–L equilibrium in the ternary solution.

A simple thermodynamic model reported earlier⁹ has been utilized in this work for the calculation of x_3^* from the partial molar volume fraction (PMVF) of solvent in the binary (solvent–CO₂) system. PMVF is defined as $(1 - X_1)\bar{v}_2/v$ and is the characteristic parameter of the binary (CO₂–expanded solvent) system in which the mole fraction of CO₂ is X_1 . PMVF is related to the molar volume, v , and partial molar volume (PMV) of the solvent \bar{v}_2 , and gives the equilibrium solubility of the solid solute, x_3^* in the ternary liquid mixture by the simple equation:

$$x_3^*(T, P) = \frac{(1 - X_1)\bar{v}_2(T, P, X_1)/v(P, X_1)}{(1 - X_{10})\bar{v}_2(T, P_0, X_{10})/v(P_0, X_{10})} \times x_{30}^*(T, P_0) \quad (6)$$

where $x_3^* = X_3^*(1 - x_1)$ and $x_1 = X_1(1 - x_3^*)$, whereas X_{30}^* is the solute mole fraction in the ternary system at the reference pressure, P_0 . X_3^* is the solid solubility in the liquid solvent (ie on the CO₂-free basis). PMVF varies between 1 and 0 as the CO₂ mole fraction in the binary mixture, X_1 varies from 0 to 1. The negative values of \bar{v}_2 intuitively indicate an extremely high degree of supersaturation in the droplet solution, as x_3^* approaches zero at $\bar{v}_2 = 0$.¹⁰ Earlier it was shown⁹ that the solubility of the cholesterol in (acetone–CO₂) solution could be predicted, in good agreement with the experimental data reported in the literature.¹¹

3.3 Rate of nucleation and critical nucleus size

Precipitation generally constitutes a two-step process. The first step is the formation of nuclei and the second is the growth of the nuclei to larger crystals. In this work only nucleation kinetics has been analysed in the solution with a high degree of supersaturation. According to the classical theory for homogeneous nucleation the free energy required for the birth of the nuclei is the sum of the free energy change for the formation of the nuclei surface and the free energy change for the transformation.¹² Thus:

$$\Delta G = \Delta G_s + \Delta G_v = 4\pi r^2 \sigma_3 + \frac{4}{3}\pi r^3 \Delta G_v \quad (7)$$

where σ_3 is the surface tension of cholesterol in the solution, which can be calculated¹³ as:

$$\sigma_3(T) = (4.105 \times 10^{-2} - 7.224 \times 10^{-5}[T - 273.15]) \quad (8)$$

The critical size of the stable nucleus is computed by minimizing the free energy with respect to the radius. Thus the critical size of the nucleus is related to the degree of supersaturation as:

$$r_c = \frac{2\sigma_3 V_m}{kT \ln S} \quad (9)$$

where V_m is the molecular volume of cholesterol.

According to the classical theory of homogeneous nucleation, the dependence of nucleation rate, \mathcal{J} , on the supersaturation ratio is given as:

$$\mathcal{J} = A \exp\left(-\frac{B}{(\ln S)^2}\right) \quad (10)$$

$$B = \left(\frac{16\pi\sigma^3 v_s^2}{3k^3 T^3}\right) \quad (11)$$

where, the pre-exponential factor, A , can be estimated by using the following relationship:

$$A = \theta \alpha_c v_s N^2 \left(\frac{2\sigma}{kT}\right)^{0.5} \quad (12)$$

where θ is the non-isothermal factor (which is 1, in the case of dilute mixtures) and α_c is the condensation coefficient (which is 0.1).¹³ N is the number of condensable molecules and is given by:

$$N = \rho_M x_3^* N_A \quad (13)$$

where N_A is the Avogadro's number, and k is the Boltzmann's constant.

4 METHODOLOGY FOR COMPUTATIONS

The process parameters, such as, pressure, temperature, flow rate of CO₂, ratio r of the volumetric flow rates of CO₂-to-solution are first selected. The degree of supersaturation is calculated at time intervals of 10^{-7} to 10^{-4} s, after ascertaining the mole fraction of CO₂ in the droplet at any instant of time.¹⁴ The following sequence of calculations is repeated:

- (i) Equations (1)–(4) are used for calculation of the number of moles of individual components in the droplet, its temperature and composition at any instant of time from the mass and heat transfer rates. The procedure for computation of mass and heat transfer coefficients is given in our earlier paper.⁷
- (ii) The Peng–Robinson equation of state is employed for calculation of the molar volume of the solution, which is then used for calculation of PMV and PMVF of solvent in the binary (CO₂–acetone) mixture in the droplet.
- (iii) Equation (6) is employed for calculation of the equilibrium mole fraction of cholesterol in the droplet at S–L equilibrium from the CO₂ mole fraction. Then t_0 (ie the time required for negligible cholesterol solubility) is obtained as the time for attaining CO₂ mole fraction for zero PMVF.
- (iv) The degree of supersaturation is calculated from the actual cholesterol mole fraction by eqn (5).
- (v) The critical nucleus diameter is computed by eqn (9), and the rate of nucleation by eqn (10).

Table 1. Physical and transport properties of CO₂ and acetone⁷

Parameter	Pressure			
	7.1 MPa	8.1 MPa	15.0 MPa	35.0 MPa
313 K				
ρ_1 (kg m ⁻³)	215.4	301.3	742.3	960.1
ρ_2 (kg m ⁻³)	685.6	684.5	696.0	706.4
D_{12}^L (m ² s ⁻¹)	7.5×10^{-9}	7.5×10^{-9}	7.1×10^{-9}	6.1×10^{-9}
D_{21}^G (m ² s ⁻¹)	4.8×10^{-8}	3.9×10^{-8}	1.5×10^{-8}	1.0×10^{-8}
σ_2 (Nm ⁻¹)	1.3×10^{-2}	1.3×10^{-2}	1.4×10^{-2}	1.5×10^{-2}
μ_1 (kg m ⁻¹ s ⁻¹)	2.2×10^{-5}	2.7×10^{-5}	0.74×10^{-5}	1.3×10^{-5}
μ_2 (kg m ⁻¹ s ⁻¹)	2.8×10^{-4}	2.9×10^{-4}	3.5×10^{-4}	3.5×10^{-4}
333 K				
ρ_1 (kg m ⁻³)		201.6		873.0
ρ_2 (kg m ⁻³)		668.7		690.2
D_{12}^L (m ² s ⁻¹)		9.3×10^{-9}		7.5×10^{-9}
D_{21}^G (m ² s ⁻¹)		5.1×10^{-8}		1.3×10^{-8}
σ_2 (Nm ⁻¹)		1.2×10^{-2}		1.4×10^{-2}
μ_1 (kg m ⁻¹ s ⁻¹)		2.2×10^{-5}		8.6×10^{-5}
μ_2 (kg m ⁻¹ s ⁻¹)		2.5×10^{-4}		3.0×10^{-4}

5 RESULTS AND DISCUSSIONS

The effects of thermodynamic states (BMCP and AMCP) and different process parameters like temperature, pressure, flow rate of CO₂, ratio of volumetric flow rates of CO₂-to-solution, and initial cholesterol mole fraction in the solution, have been analyzed on the degree of supersaturation, critical nucleus diameter, and rate of nucleation up to t_0 , the time for attaining zero cholesterol solubility in the droplet solution during its flight in the flowing SC CO₂ environment. The simulation has been performed in the pressure range of 7.1–35.0 MPa, the temperature range of 313–333 K, the SC CO₂ flow rate range of 0.1136–1.136 mol s⁻¹, the range of the ratio r of 100–1000, and X_{30} range of 0.0025–0.010 (saturated solution). The initial droplet diameter has been calculated from the hydrodynamics of the solution and CO₂ streams being sprayed through concentric nozzles of 50 μ m and 70 μ m respectively. The in-flight diameter has been evaluated up to t_e , the time required for complete extraction of acetone at different process conditions and have been reported earlier.⁷ The physical and transport properties of SC CO₂ and acetone are listed in Table 1, the critical constants in Tables 2 and 3 and the properties of cholesterol in Table 4.

Table 2. Critical properties of CO₂ and acetone⁷

Component	T_c (K)	P_c (MPa)	ω
CO ₂ (1)	304.2	7.38	0.225
Acetone(2)	508.1	4.70	0.304

Table 3. Interaction constants and MCP for CO₂-acetone system⁷

Component	k_{12}	l_{12}	P_{cm} (Mpa)
313 K	-0.007	0.002	8.23
333 K	-0.062	0.0015	8.72

Table 4. Properties of cholesterol⁸

Δh^f (kJ mol ⁻¹)	T_m (K)	Relative molecular mass	Molar volume (g cm ⁻³)
304.2	421.7	386.67	1.0674

The solubility of cholesterol in acetone at different temperatures, at the reference pressure P_0 is required for the calculation of the equilibrium mole fraction of cholesterol in solution from the PMVF of solvent⁹ and has been obtained from the interpolated experimental data reported by Prausnitz *et al*⁸ as listed in Table 5. The solubility of cholesterol in liquid phase decreases with an isobaric increase in CO₂ mole fraction much faster at 333K than at 313 K due to the antisolvent effect, as can be seen from Fig 2, indicating a faster rate of supersaturation attained at the higher temperature. However the solubility of cholesterol at the lower temperature of 313 K may exceed that at 333 K at 8.1 MPa (which is not observed at 35.0 MPa) for high values of CO₂ mole fraction. This is similar to the ‘crossover phenomenon’ observed in the solubility behaviour in SC CO₂ at lower pressures.

5.1 Supersaturation

5.1.1 Effect of pressure

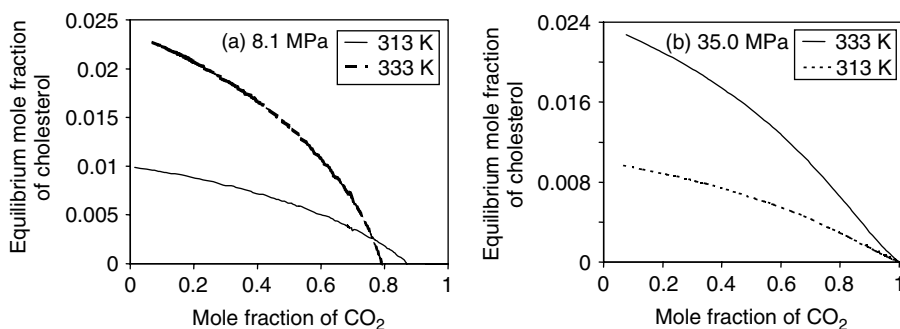
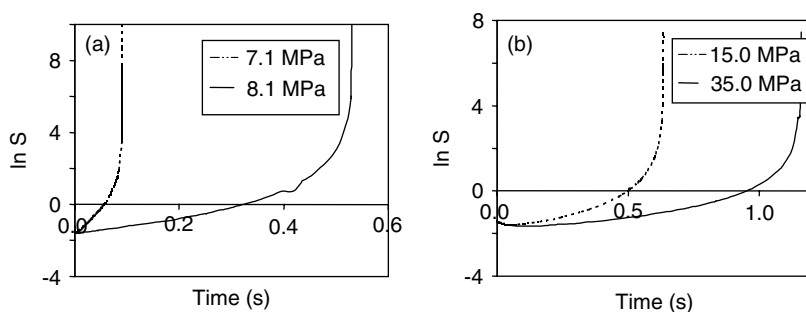
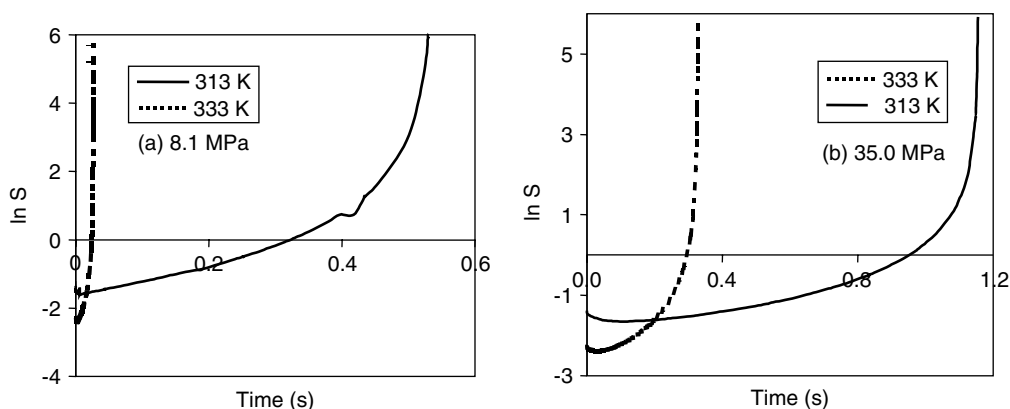
The effect of pressure on the increase in the degree of supersaturation with time can be seen from Fig 3 in the two thermodynamic states of BMCP (Fig 3(a))

Table 5. Solubility of cholesterol in acetone at two temperatures and $P_0 = 0.1$ MPa⁸

Temperature (K)	X_{30}^* or x_{30}^*
313	0.010
333	0.0237

Table 6. Effect of thermodynamic states on supersaturation and nucleation rates, and critical nucleus size at $m_{\text{CO}_2} = 0.1136 \text{ mol s}^{-1}$, $r = 500$ and $X_{30} = 0.0025$

Temp (K)	Pressure (MPa)	t_e (s) at $x_2 = 0$ (t_0 (s) at $x_3^* = 0$)	Time(s) for $\ln S = 5$	r_c (nm) at $\ln S = 5$	J at $\ln S = 5$ (nuclei $\text{m}^{-3} \text{s}^{-1}$)
313	7.1	0.26(0.09)	0.01	2.10	3.65×10^{20}
	8.1	0.53(0.53)	0.53	2.10	3.65×10^{20}
	15.0	0.79(0.66)	0.63	2.15	3.65×10^{20}
	35.0	1.16(1.16)	1.15	2.15	3.65×10^{20}
333	8.1	0.06(0.028)	0.03	1.85	1.47×10^{26}
	35.0	0.33(0.33)	0.33	1.85	1.47×10^{26}

**Figure 2.** Effect of temperature on equilibrium solubility of cholesterol in CO_2 -acetone mixture at (a) 8.1 MPa and (b) 35.0 MPa.**Figure 3.** Effect of pressure on $\ln S$ for (a) BMCP and (b) AMCP at 313 K, $m_{\text{CO}_2} = 0.114 \text{ mol s}^{-1}$, $r = 500$, $X_{30} = 0.0025$.**Figure 4.** Effect of temperature on $\ln S$ for (a) BMCP and (b) AMCP for $m_{\text{CO}_2} = 0.114 \text{ mol s}^{-1}$, $r = 500$, $X_{30} = 0.0025$.

and AMCP (Fig 3(b)). It is faster and higher at a lower pressure in either BMCP or AMCP. This is due to the fact that a lower value of x_3^* is observed at a lower pressure for a particular mole fraction of CO_2 in the solution and also a higher and faster decrease

in x_3^* with mole fraction of CO_2 in the CO_2 -acetone solution. Accordingly, t_0 has the lowest value at the lowest pressure of BMCP and the isothermal degree of supersaturation increases faster at a lower pressure, as can be seen from Table 6.

5.1.2 Effect of temperature

The effect of temperature on the increase in the degree of supersaturation with time can be seen from Fig 4 in the two thermodynamic states of BMCP (Fig 4(a)) and AMCP (Fig 4(b)). There is a 'crossover phenomenon' observed in the behaviour of equilibrium cholesterol solubility, x_3^* , and consequently the degree of supersaturation, owing to two opposite effects of temperature, namely (i) a lower value of x_3^* is observed for a particular mole fraction of CO₂ at the higher temperature due to the negative effect of temperature on PMVF and (ii) there is a positive effect of temperature on x_{30}^* , the solubility of cholesterol at the reference pressure P_0 . The decrease in x_3^* with CO₂ mole fraction is higher at the higher temperature of 333K. For example, a value of 5 for $\ln S$ is attained faster at the higher temperature for a given pressure, for which t_e and t_0 are also lower (also, $t_e > t_0$), as can be seen from Table 6. The rate of increase of the degree of supersaturation is extremely large due to a very rapid reduction of x_3^* to zero within very low values of time, t_0 , at which the degree of supersaturation theoretically attains infinity. Thus a higher temperature is desirable for a faster and higher degree of supersaturation.

5.1.3 Effect of CO₂ flow rate

An increase in the CO₂ flow rate results in a higher convective mass transfer rate due to a higher CO₂

velocity, which in turn entails a higher rate of extraction of solvent from the droplet. This, in turn, causes a faster reduction in x_3^* to zero, resulting in lower values of t_0 and hence a faster and higher degree of supersaturation as can be seen from Fig 5 for BMCP (Fig 5(a)) and AMCP (Fig 5(b)). Thus a higher CO₂ flow rate at a constant value of r gives a higher and faster degree of supersaturation.

5.1.4 Effect of volumetric flow ratio

A lower ratio of CO₂-to-solution volumetric flow rates at a constant CO₂ flow rate implies a higher solution flow rate, which causes atomization to a smaller initial droplet size and high convective mass transfer of CO₂. This ultimately results in a faster reduction in x_3^* to zero, resulting in lower values of t_0 at a lower value of r . Accordingly a higher solution flow rate causes a higher and faster degree of supersaturation, as can be seen from Fig 6 for BMCP (Fig 6(a)) and AMCP (Fig 6(b)).

5.1.5 Effect of initial solution concentration

As can be seen from Fig 7, the degree of supersaturation is higher in the saturated solution at any time than in the dilute solution for BMCP (Fig 7(a)) and AMCP (Fig 7(b)). It is interesting to note that t_0 is lower in the saturated solution for BMCP, whereas t_0 for both initial solution concentrations coincides for AMCP.

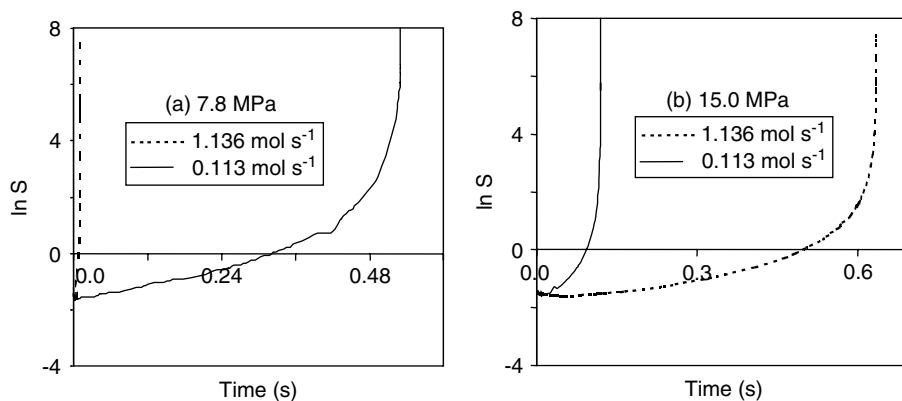


Figure 5. Effect of CO₂ flow rate on $\ln S$ for (a) BMCP and (b) AMCP at 313K, $r = 500$ and $X_{30} = 0.0025$.

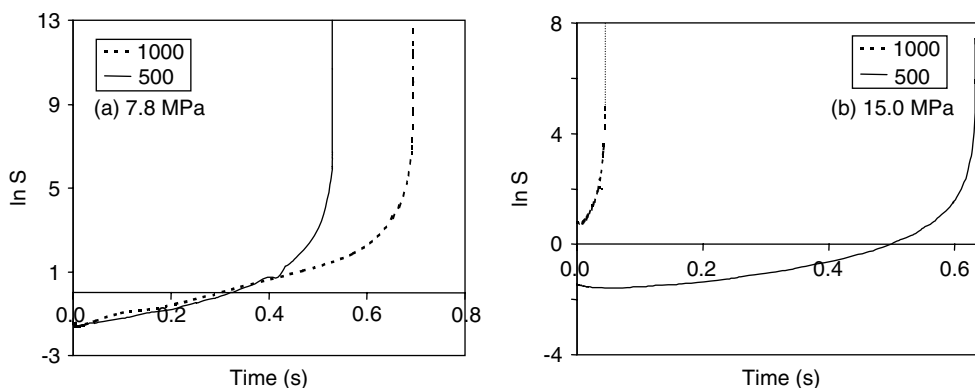


Figure 6. Effect of r on $\ln S$ for (a) BMCP and (b) AMCP at 313K, $m_{CO_2} = 0.114 \text{ mol s}^{-1}$ and $X_{30} = 0.0025$.

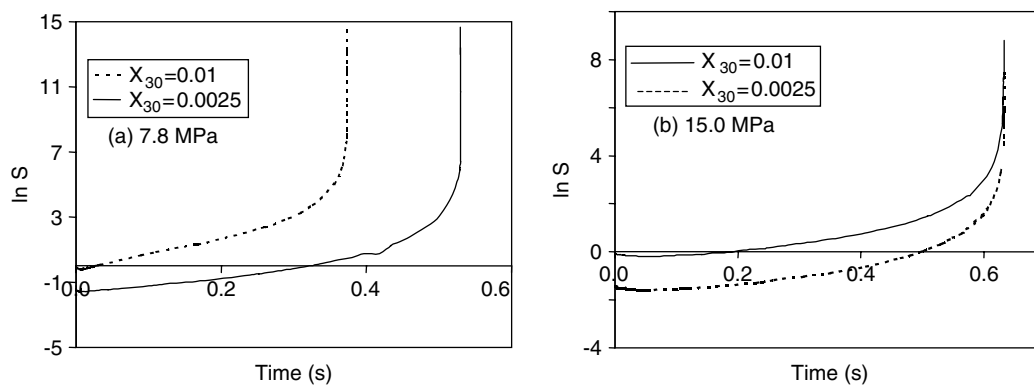


Figure 7. Effect of X_{30} on $\ln S$ for (a) BMCP and (b) AMCP at 313 K, $m_{\text{CO}_2} = 0.114 \text{ mol s}^{-1}$ and $r = 500$.

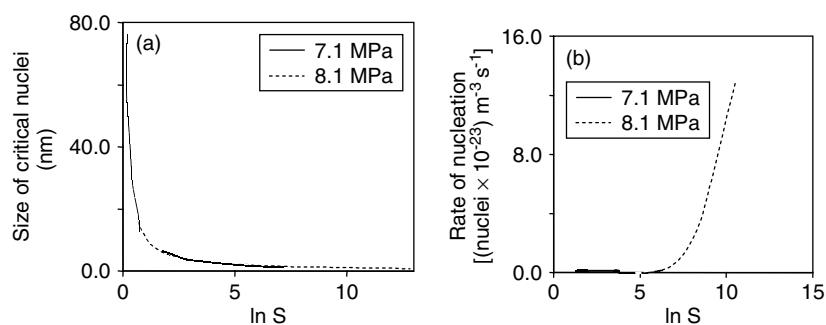


Figure 8. Effect of pressure on (a) r_c and (b) nucleation rate at BMCP for 313 K, $m_{\text{CO}_2} = 0.114 \text{ mol s}^{-1}$, $r = 500$, $X_{30} = 0.0025$.

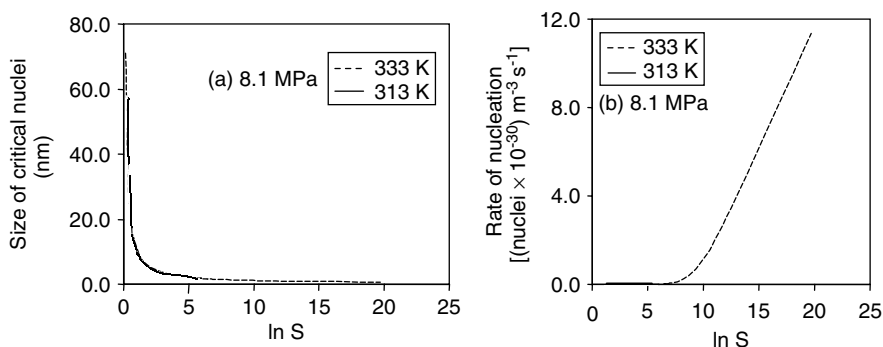


Figure 9. Effect of temperature on (a) r_c and (b) nucleation rate at BMCP for $m_{\text{CO}_2} = 0.114 \text{ mol s}^{-1}$, $r = 500$, $X_{30} = 0.0025$.

Thus a higher solution concentration is required for a faster and higher degree of supersaturation.

5.2 Nucleation

5.2.1 Effect of pressure

The size of the critical nucleus and the rate of nucleation depend solely on the degree of supersaturation, in either thermodynamic states of BMCP or AMCP and accordingly the effects of pressure on supersaturation and nucleation kinetics are similar. The size of the critical nucleus formed asymptotically decreases as the degree of supersaturation increases. It ranges from 1.0 to 0.1 nm at very high supersaturation as $\ln S$ attains a value in the range of 5–6, as can be seen from Fig 8(a). The nucleation rate sharply increases with the degree of supersaturation at high values (ie at time nearing t_0), as can be seen

from Fig 8(b). The nucleation rate and critical size of the nucleus remain almost invariant with pressure at a given degree of supersaturation and temperature, as can be seen from Table 6. A faster nucleation rate results in a smaller critical nucleus size and eventually smaller nanoparticles. Chattopadhyay and Gupta¹⁵ experimentally verified this fact, as it was observed that the particle size increased with pressure or density. Subra and Vega¹¹ also recently reported a decrease in the final particle size with decrease in pressure for precipitation of cholesterol from its solution in methylene chloride. This may be attributed to a higher degree of supersaturation and higher nucleation rates with a decrease in pressure or density.

5.2.2 Effect of temperature

As mentioned earlier, the size of the critical nucleus depends upon the supersaturation attained, as can be

seen from Fig 9(a), and there is no difference in the behaviour of their inter-dependence at two temperatures for both BMCP and AMCP. The nucleation rate is higher at the higher temperature at the same level of supersaturation, which can be seen from Fig 9(b) with a monotonous increase in the rate of nucleation with the degree of supersaturation. As can be seen from eqn (12), the higher the temperature and the higher the supersaturation attained, the faster and the higher is the nucleation. As can be seen from Table 6, the nucleation rate increases with temperature at a given value of supersaturation vis-à-vis the induction time and critical nucleus size decrease. Thus a higher temperature ultimately gives rise to rapid nucleation, which then results in a large number of stable nuclei of smaller critical nucleus size, and hence in nanoparticles of a smaller size. This was experimentally verified by Chattopadhyay and Gupta¹⁵ for production of fullerene particles and by Thiering *et al*¹⁶ for the SAS precipitation of proteins respectively, as it was observed that the particle size decreased with an increase in temperature at a constant pressure.

5.2.3 Effect of CO₂ flow rate

As explained earlier, the critical size of the nucleus depends solely on the degree of supersaturation and there is no difference in the behaviour of its dependence on flow rates of CO₂, r , and initial solution concentrations. The rate of attainment of supersaturation is higher at a higher CO₂ flow rate, which causes a higher rate of nucleation. The critical nucleus size asymptotically decreases from 10 nm to 0.1 nm with increasing degree of supersaturation at $\ln S > 5$, as can be seen from Fig 10(a). Hence a higher CO₂ flow rate is favourable for a smaller critical nucleus.

5.2.4 Effect of volumetric flow ratio

A lower flow ratio implies a higher solution flow rate, and a higher and faster attainment of supersaturation due to greater atomization to a smaller initial droplet diameter and a higher mass transfer of CO₂. A lower flow ratio r results in a higher rate of nucleation due to attainment of a higher degree of supersaturation. The critical nucleus size decreases asymptotically from 10 nm to 0.1 nm with increasing degree supersaturation, as can be seen from Fig 10(b) at high supersaturation (at $\ln S > 5$). This was experimentally verified by Magnan *et al*¹⁷ for production of phospholipid particles and by Chattopadhyay and Gupta¹⁵ for production of fullerene particles as it was observed that the particle size decreased with an increase in the solution flow rate.

5.2.5 Effect of initial solute concentration

As can be seen from Fig 10(c) the critical nucleus size decreases asymptotically with the degree of supersaturation from 1 nm to 0.01 nm at $\ln S > 5$ and there is hardly any effect of initial solute concentration in the solution. The critical nucleus size, drastically

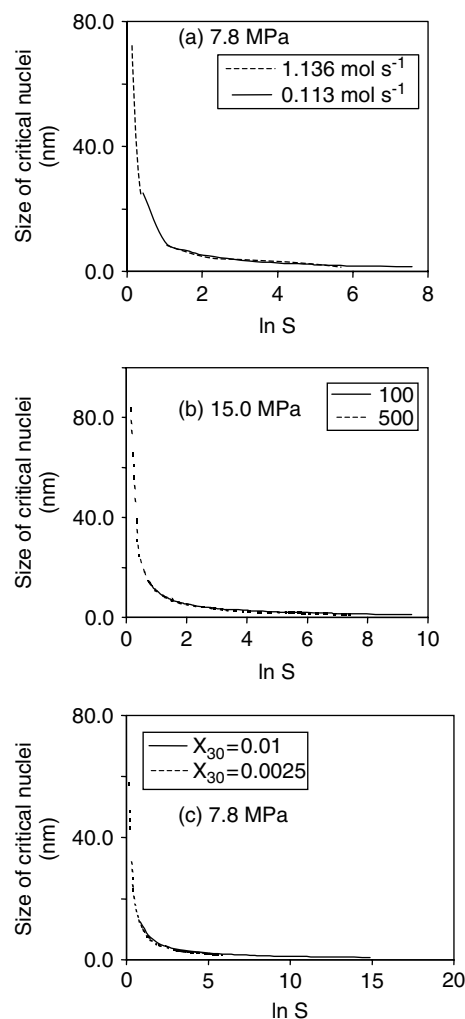


Figure 10. Effects of various process parameters on variation of critical nucleus size vs $\ln S$: (a) m_{CO_2} at 313 K, $r = 500$, $X_{30} = 0.0025$; (b) r at 313 K, $m_{\text{CO}_2} = 0.114 \text{ mol s}^{-1}$, $X_{30} = 0.0025$; (c) X_{30} at 313 K, $m_{\text{CO}_2} = 0.114 \text{ mol s}^{-1}$, $r = 500$.

decreasing with increasing degree of supersaturation, leads to the formation of nanoparticles.

6 CONCLUSIONS

The paper presents an analysis of the effects of various process variables on the degree of supersaturation, critical nucleus diameter, and rate of nucleation. It can be concluded that it is desirable to operate the SAS process at a higher temperature and a lower pressure in the thermodynamic state of BMCP with higher flow rates of CO₂ and solution (in the ranges of the process parameters studied in this work), in order to attain a higher and faster degree of supersaturation. The behaviour of dependencies of the size of the critical nucleus and nucleation rate on the process variables are similar to that of supersaturation. The time, t_e for complete extraction of solvent, is higher or almost equal to the time, t_0 for attaining a negligible value of x_3^* or an infinitely large degree of supersaturation that can be theoretically attained in the droplet solution. The supersaturation and nucleation rates are very high

as time approaches t_0 , and t_0 is lower for a higher flow rate of CO_2 at a lower pressure, higher temperature and BMCP. The degree of supersaturation, as high as $\ln S > 5$ at 333 K, causes nucleation rates of the order of 10^{26} nuclei $\text{m}^{-3} \text{sec}^{-1}$ and the critical nucleus size of the order of 1 nm or less. There are hardly any effects of pressure, flow rates of CO_2 and solution, and initial solute concentration on the dependencies of the degree of supersaturation on nucleation rate and critical nucleus size at any temperature. The rate of attainment of supersaturation is higher and t_0 is lower (for BMCP) in the saturated solution at any time than in the dilute solution, though t_0 remains the same for both concentrations at AMCP. So the faster the degree of supersaturation and the higher the temperature, the higher is the nucleation rate and the smaller is the size of the critical nucleus for precipitation of cholesterol from acetone solution by the SAS process.

REFERENCES

- Palakodaty S and York P, Phase behavioral effects on particle formation processes using supercritical fluids. *Pharmaceutical Research* **16**:976–985 (1999).
- Mukhopadhyay M and Dalvi SV, A new thermodynamic method for solid–liquid–vapor equilibrium in ternary systems from binary data for antisolvent crystallization, in *Proc of the 6th International Symposium on Supercritical Fluids*. Versailles, France, April, pp 717–721 (2003).
- Bristow S, Shekunov T, Shekunov BY and York P, Analysis of supersaturation and precipitation process with supercritical CO_2 . *Journal of Supercritical Fluids* **21**:257–271 (2001).
- Shekunov BY, Baldyga J and York P, Particle formation by mixing with supercritical antisolvent at high Reynolds number. *Chemical Engineering Science* **56**:2421–2433 (2001).
- Werling J and Debenedetti PG, Numerical modeling of mass transfer in the supercritical antisolvent process: miscible conditions. *Journal of Supercritical Fluids* **18**:11–24 (2000).
- Werling J and Debenedetti PG, Numerical modeling of mass transfer in the supercritical antisolvent process. *Journal of Supercritical Fluids* **16**:167–181 (1999).
- Mukhopadhyay M and Dalvi SV, Mass and heat transfer analysis of SAS: effects of thermodynamic states and flow rates on droplet size. *Journal of Supercritical Fluids* **30**:333–348 (2004).
- Prausnitz JM, Lichtenthaler RN and de Azevedo EG, *Molecular Thermodynamics of Fluid Phase Equilibria*, 3rd edn. Prentice Hall Inc, New Jersey (1999).
- Mukhopadhyay M and Dalvi SV, Partial molar volume fraction of solvent in binary (CO_2 –solvent) solution for solid solubility predictions. *Journal of Supercritical Fluids* **29**:221–230 (2004).
- Mukhopadhyay M, Partial molar volume reduction of solvent for solute crystallization using carbon dioxide as antisolvent. *Journal of Supercritical Fluids* **25**:213–223 (2003).
- Subra P and Vega A, Crystallization in CO_2 medium: from phase equilibria to products, in *Proc of the 6th International Symposium on Supercritical Fluids*. Versailles, France, April. Vol 3, pp 1629–1634 (2003).
- Myerson AS, *Handbook of Industrial Crystallization*, 2nd edn. Butterworth Heinemann, MA, USA, pp 43–46 (2001).
- Turk M, Influence of thermodynamic behavior and solute properties on homogeneous nucleation in supercritical solutions. *Journal of Supercritical Fluids* **18**:169–184 (2000).
- Dalvi SV, Mathematical modeling of supercritical antisolvent crystallization. M Tech Dissertation, Indian Institute of Technology, Bombay, India (2003).
- Chattopadhyay P and Gupta R, Supercritical CO_2 based production of fullerene nanoparticles, in *Proc of the 5th International Symposium on Supercritical Fluids*, Atlanta, USA (2000).
- Thiering R, Dehghani F and Foster NR, Micronization of model proteins using compressed carbon dioxide, in *Proc of the 5th International Symposium on Supercritical Fluids*, Atlanta, USA (2000).
- Magnan C, Badens E, Commenges G and Charbit G, Soy lecithin micronization with a compressed fluid antisolvent—influence of process parameters. *Journal of Supercritical Fluids* **19**:69–77 (2000).